Biphoton spectral quantum interference for information processing and delay metrology

Suparna Seshadri^a, Hsuan-Hao Lu^b, Joseph M. Lukens^{b,c}, and Andrew M. Weiner^a

 ^aSchool of Electrical and Computer Engineering and Purdue Quantum Science and Engineering Institute, Purdue University, West Lafayette, Indiana 47907, USA
 ^bQuantum Information Science Section, Oak Ridge National Laboratory, Oak Ridge, Tennessee 37831, USA

^cResearch Technology Office, Arizona State University, Tempe, Arizona 85287, USA

ABSTRACT

Broadband time-energy entangled photons feature strong temporal correlations with potential for precision delay metrology, but previous work has leveraged only time-of-flight information ultimately limited by the detection jitter and resolution of the time-tagging electronics. Firstly, our work pushes the entanglement-based nonlocal delay metrology from the conventional time-of-flight measurement to a new direction—two-photon interferometry with subpicosecond sensitivity independent of detection resolution. Next, we show the selective sensitivity of frequency-bin encoded Bell states to the sum and difference of biphoton-delays by using a novel reconfigurable setup capable of switching between the Bell states by successively employing single and dual spectral-line pumps.

Keywords: Time-energy entanglement, delay metrology, two-photon interferometry, frequency-bin encoded Bell states.

1. INTRODUCTION

Measurements of strong temporal correlations in entangled photons have been explored as a means for timing synchronization and positioning in quantum networks.¹⁻⁵ Additionally, in LiDAR and imaging applications, time-of-flight (ToF) coincidence measurements have been identified as robust and secure in complex adversarial and noisy environments.⁶⁻¹⁰ Traditionally, biphoton ToF measurements involve recording the time at which they reach single-photon detectors. However, the accuracy of this method is limited by the inherent jitter in the detectors and the precision of the timing equipment used.⁵⁻⁹ Although entangled photons can be generated over terahertz-scale bandwidths with subpicosecond features in their temporal correlations, commercially available single photon detectors suffer from jitters on the order of tens of picoseconds and so cannot resolve them. Here, we describe and demonstrate a scheme that exploits broadband phase modulation to overcome the limitations posed by the detector jitter. Our scheme can detect small delay changes by mapping the joint spectral phase of the biphoton wavepacket to coincidence probabilities. This technique draws inspiration from earlier research on spectral phase coherence in high-dimensional frequency bin-entangled photons and uses electro-optic phase modulation for coherent frequency mixing. 11-15 Instead of manipulating spectral phase to violate Bell's inequality, for example, our method measures changes in spectral phase to determine the difference in arrival time between the signal and idler photon. The measurement is made possible by sinusoidal radio-frequency (RF) phase modulation, which allows for a generalized delay to be measured without requiring local overlap of the signal and idler, which can travel along separate paths.

In this paper, we first describe our method for measuring biphoton delays in an interferometric setup and present recently published proof-of-principle results. ¹⁶ We show that our scheme can complement nonlocal ToF measurements of biphotons while resolving features that are otherwise lost due to detection jitter. In the second half of the paper, we examine the sensitivity of different frequency-bin Bell states to biphoton delay shifts. We summarize a novel scheme first proposed in Ref. 17 for generating all four frequency-bin Bell states and investigate how they respond to the sum and difference of signal-idler delays.

Corresponding author: A.M.W.: amw@purdue.edu

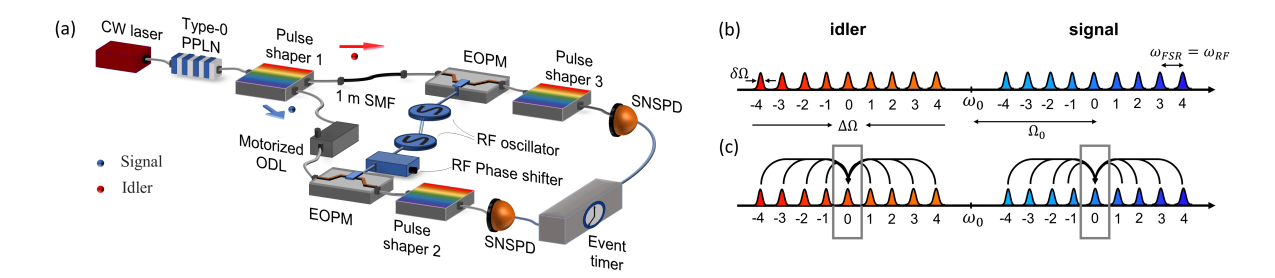


Figure 1. (a) Experimental setup for nonlocal delay metrology. CW laser: continuous-wave laser, PPLN: periodically poled lithium niobate waveguide, ODL: optical delay line, SMF: single-mode fiber, EOPM: electro-optic phase modulator, SNSPD: superconducting nanowire single-photon detector. (b) Pictorial representation of nine-dimensional biphoton frequency comb in the frequency domain. (c) Phase-modulation-induced contributions from all sidebands to the pair of frequency bins $|0,0\rangle_{SI}$ selected for coincidence detection.

2. DELAY METROLOGY THROUGH NONLOCAL MODULATION

Figure 1 illustrates the experimental setup and the frequency-domain representation of the delay sensing scheme. The Fourier transform relationship between the biphoton wavefunction in the frequency and delay bases lays the foundation for the sensing technique. The scheme entails nonlocal phase modulation in the optical links traversed by the biphotons, where the modulation depth is sufficiently strong to produce sidebands filling roughly half of the optical bandwidth, thus causing all signal and idler frequency bins to interfere in their respective central frequency bins (given by $|0,0\rangle_{SI}$), which are selected by spectral filters and detected. The interference of the sidebands maps the joint spectral phase of the biphotons to the probability of coincidence detection. This coincidence probability is closely linked to the inverse Fourier transform of the biphoton spectral amplitude, where the time variable is the difference in generalized delays, represented as $\tau = (\tau_S + \phi_S \omega_{\rm FSR}^{-1}) - (\tau_I + \phi_I \omega_{\rm FSR}^{-1})$, where $\omega_{\rm FSR}$ refers to the separation between the different frequency bins of the biphoton frequency comb. The variables τ_S and ϕ_S respectively represent the time of arrival of the signal photon at the phase modulator and the RF phase of the modulation waveform with reference to a global clock, with τ_I and ϕ_I being the equivalent measures for the idler.

2.1 Theory

Consider the input biphoton state with 2N+1 frequency bins in the signal and idler spectra,

$$|\Psi\rangle = \sum_{k=-N}^{N} \alpha_k |k, -k\rangle_{SI}, \qquad (1)$$

where, $|k,-k\rangle_{SI}$ represents the state of a frequency-bin pair with the signal photon occupying the $k^{\rm th}$ signal bin and idler photon occupying the $-k^{\rm th}$ idler bin at center frequencies $\omega_0 + \Omega_0 + k\omega_{\rm FSR}$ and $\omega_0 - \Omega_0 - k\omega_{\rm FSR}$ respectively, where Ω_0 is the frequency offset from the pump half-frequency ω_0 . The complex spectral amplitude of the $k^{\rm th}$ bin-pair is represented as α_k . On continuous-wave pumping of the nonlinear parametric process, $|k,-k\rangle_{SI}$ can be represented as $\int d\Omega \ f(\Omega - (\Omega_0 + k\omega_{FSR})) \ |\omega_0 + \Omega\rangle_S \ |\omega_0 - \Omega\rangle_I$, where $f(\Omega)$ is a lineshape function. After the signal and idler travel through their respective links, sinusoidal phase modulation is applied on both, of the form $e^{-im\sin(\omega_{\rm FSR}\,t+\phi_S)}$ and $e^{-im\sin(\omega_{\rm FSR}\,t+\phi_I)}$ respectively. The central frequency bins $|0,0\rangle_{SI}$ are measured and the coincidence probability takes the form 16

$$\mathcal{P}(\tau) \propto \left| \sum_{k=-N}^{N} \alpha_k C_k e^{ik\omega_{\text{FSR}}\tau} \right|^2.$$
 (2)

Here, $\tau = (\tau_S - \tau_I) + \omega_{\text{FSR}}^{-1}(\phi_S - \phi_I)$ is the generalised differential delay, the coefficient $C_k = J_k(m)J_{-k}(m) = (-1)^k J_k^2(m)$ results from the phase modulation sidebands, $J_k(m)$ is the Bessel function of the first kind, and m

is the modulation index in radians. Thus the coincidence probability is the squared magnitude of the inverse Fourier transform of the complex spectral amplitudes weighted by the mixing coefficients C_k .

2.2 Setup

We demonstrate a basic implementation of the interferometric sensing scheme, complemented with detection time tags, to measure the delay introduced by a 1 m-long single-mode fiber (SMF) with subpicosecond precision. A continuous-wave laser at 778 nm with ~ 200 kHz linewidth pumps a fiber-pigtailed periodically poled lithium niobate (PPLN) ridge waveguide designed for type-0 phase matching to generate time-energy entangled photons. The biphotons cover >5 THz centered at 1556 nm. Signal and idler spectra are selected by a programmable pulse shaper (pulse shaper 1) with a width of $\Delta\Omega/2\pi = 190$ GHz and offset $\Omega_0/2\pi = 200$ GHz. The signal and idler are routed to different optical links, and an electro-optic phase modulator (EOPM) is placed at the end of each link driven at frequency $\omega_{\text{FSR}}/2\pi = 20$ GHz and modulation depth of m = 4.48 rad. This allows sidebands from effectively nine frequency bins in each of the signal and idler spectra to contribute coherently to the central frequency bin as shown in Fig. 1(c). A pulse shaper after each EOPM selects the central frequency bin and routes it to superconducting nanowire single photon detectors (SNSPDs) in each of the signal and idler arms. The combined timing jitter of the SNSPDs is ~100 ps. An optical delay line (ODL) located in the signal arm before the EOPM is adjusted in increments of 0.4 ps, and at each step, the total number of coincidences are recorded over five seconds, resulting in an interferogram as a function of the ODL setting $\Delta \tau_{\circ}$. These interferograms are recorded with and without a 1 m SMF patch cord placed in the idler arm; results normalized to a peak of unity are plotted in Fig. 2(a,b). The relative RF phase of the sinusoidal moduation waveforms are unaltered during these measurements, and the ODL settings are referenced to the same starting point $\Delta \tau_s = 0$. Example raw histograms (acquired at the ODL settings where the peaks in the interferograms occur) are overlayed in Fig. 2(c), both for the cases with and without the 1 m SMF; curves like these are what are integrated to produce each individual point in Fig. 2(a,b).

2.3 Results and discussion

As predicted by Eq. (2), the interferograms repeat every $T_{\rm rep} = 50$ ps, limited only by the coherence length of the biphotons. Experimentally, the coherence time is 5 µs, determined by the reciprocal of the pump linewidth, which is equivalent to an imbalance of 1 km in standard fiber. On insertion and removal of additional delays represented by $\Delta \tau_I$ due to the SMF in the idler arm, the corresponding interferograms shift by $\Delta \tau_I$ modulo 50 ps. This is because the two interferograms in Fig. 4(a) and (b) can each be viewed as part of longer \sim 5 µs-wide interferograms under which all features repeat at multiples of $T_{\rm rep}$. The true delay due to the SMF is therefore,

$$\Delta \tau_I = kT_{\text{rep}} - (\Delta \tau_S^{(\text{w/o})}(P_j) - \Delta \tau_S^{(\text{w/})}(P_i)) \qquad k \in \mathbb{Z}, i \in \{1, 2\}, j \in \{3, 4\}.$$
 (3)

where $\Delta \tau_S^{(\mathrm{w/o})}(P_i)$ and $\Delta \tau_S^{(\mathrm{w/o})}(P_j)$ are settings of the signal ODL arm where an interference peak occurs, in the presence and absence of the additional SMF, respectively. The integer k is the (initially unknown) number of repetition periods between the absolute positions of P_j and P_i , an ambiguity that can be removed by examining the raw histograms in a traditional ToF sense. For instance, consider peaks P_4 and P_2 in Fig. 2(c); the difference in means of the Gaussian fits is 5002 ps with a 95% confidence spread of 6 ps. Hence the value k = 100 can be recovered. Then, from the fits to the interferograms [Fig. 2(a,b)], the offset in ODL settings at peaks P_4 and P_2 is $\Delta \tau_S^{(\mathrm{w/o})}(P_4) - \Delta \tau_S^{(\mathrm{w/o})}(P_2) = -14.65 \pm 0.04$ ps. From Eq. (3), the effective delay introduced due to the 1 m SMF is therefore 5014.65 \pm 0.04 ps—consistent within manufacturer specifications. The estimate is identical for all the pairs of peaks in Fig. 2(a,b).

In sum, we have demonstrated a scheme where spectral interference using phase modulation can be used to improve the resolution of ToF measurements when the bandwidth supported by the modulator exceeds that which can be resolved by the single-photon detectors. We accomplish in resolving picosecond-scale temporal correlation features in a nine-dimensional \sim 190 GHz bandwidth biphoton frequency comb by acquiring an two-photon coincidence interferogram with an precision of 0.04 ps in sensing changes to difference in biphoton delays.

While our approach is complemented with time tags from SNSPDs with ~ 100 ps jitters, the scheme can also aid ToF measurements with nanosecond-scale jitters if the repetition period $T_{\rm rep}$ of the modulating waveform is suitably increased. One technique to increase the modulation period while still maintaining the fine resolution

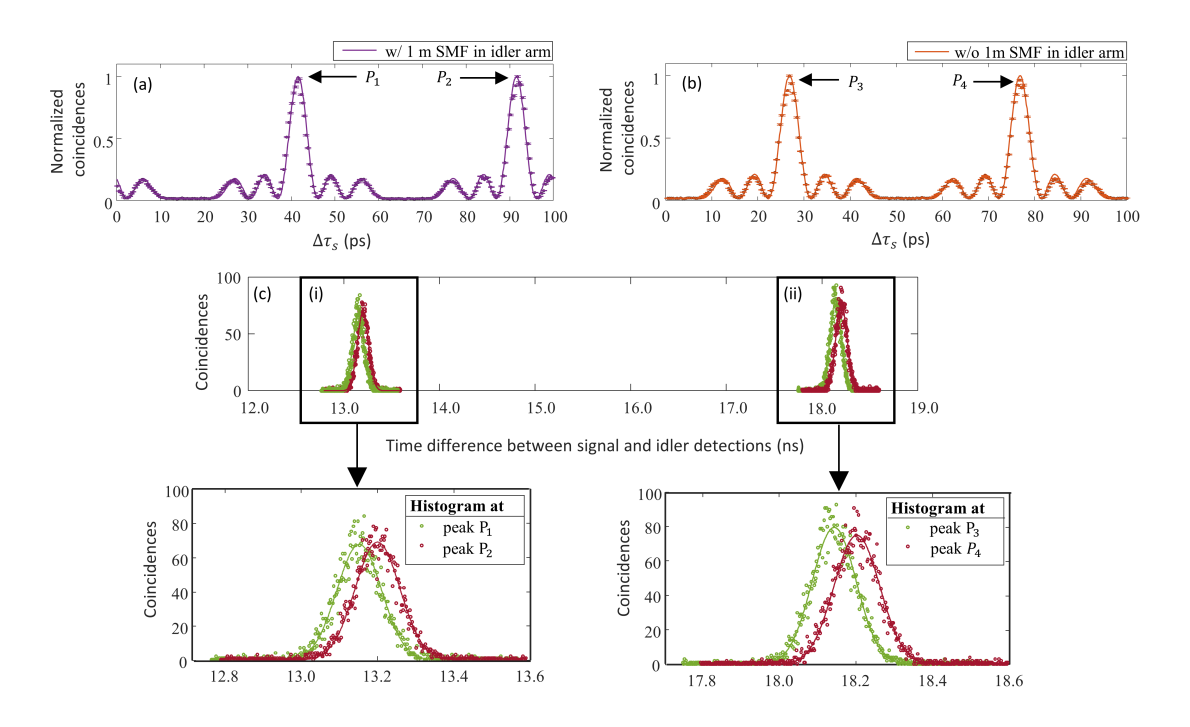


Figure 2. Interferograms measuring two-photon coincidences that were recorded (a) with and (b) without a 1 m-long SMF in the idler arm. Solid lines: Theoretical coincidence probability which is normalized and fit to the experimental curves. (c) Histograms of coincidences acquired when the ODL in the signal arm is set to the delay positions corresponding to the datapoints at peak P_1 and P_2 from (a), and P_3 and P_4 from (b). The time bins in the histograms are 2 ps wide. Solid lines are Gaussian fits.

from high bandwidth could use two very closely (megahertz-scale) spaced sinusoidal waveforms. The modulation period here is determined by the difference in the frequencies of the two sinusoids while the their absolute frequencies can still be on the order of tens of GHz. We note that this is similar to distance measurements using classical dual frequency combs where slightly different repetition rates are known to offer long-range sensing as well as high resolution. ^{18,19} The presented approach for nonlocal delay metrology has further capabilities ¹⁶ including sensitivity to relative RF modulation phase as indicated in the theory as well as robustness to imbalance in the path lengths of biphotons (up to the biphoton coherence length). As technologies for both modulation and single-photon detection continue to improve and support higher bandwidths, it is yet to be determined which of these will ultimately surpass the other. Irrespective of this outcome, a suitable measurement scheme can be selected to best utilize the full optical bandwidth available in ToF measurements.

3. DELAY SENSITIVITY OF FREQUENCY-BIN BELL STATES

Bell states are a valuable resource for investigating the fundamental principles of quantum entanglement and for realizing practical outcomes in quantum information processing and metrology. They are widely used in a variety of quantum communication protocols, including dense coding, teleportation, cryptography, and entanglement swapping. Furthermore, Bell states can play a crucial role in quantum metrology. The ability to generate all four frequency-bin-encoded Bell states would enable advanced capabilities for delay sensing, such as nonlocal measurements and a two-photon advantage in resolution. While the results presented so far demonstrate nonlocal sensing of differential delay by using negative frequency correlations in the biphoton state, in this section we juxtapose them with the possibilities offered by positive-frequency-correlated states. To demonstrate this, we introduce a new technique for producing all four frequency-bin Bell states from spontaneous parametric down-conversion (SPDC) by manipulating the pump spectrum. We use spectral mixing and filtering to examine the complementary sensitivities of the Bell states to the sum and difference in delays traversed by the biphotons.¹⁷

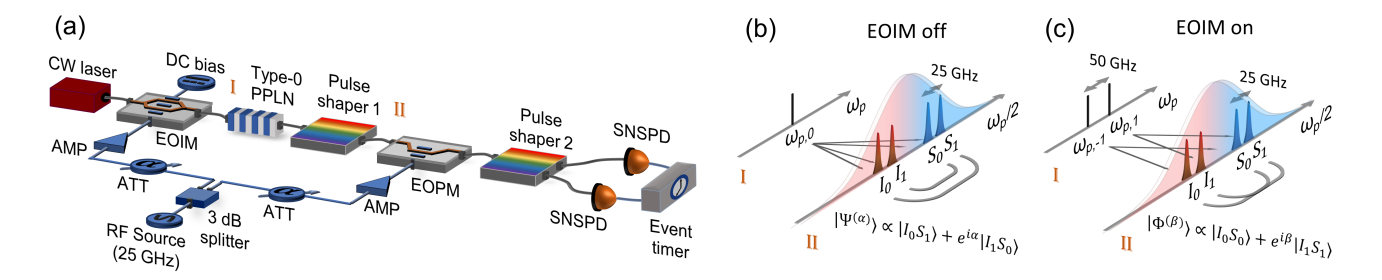


Figure 3. (a) Experimental setup for Bell state generation. CW laser: continuous-wave laser, EOIM: Electro-optic intensity modulator, AMP: RF Amplifier, ATT: variable RF attenuator, EOPM: Electro-optic phase modulator, SNSPD: Superconducting nanowire single photon detector. Frequency domain illustration for the generation of (b) $|\Psi^{(\alpha)}\rangle$ - and (c) $|\Phi^{(\beta)}\rangle$ -type states.

The Bell states are defined as $|\Psi^{\pm}\rangle \propto |01\rangle \pm |10\rangle$ and $|\Phi^{\pm}\rangle \propto |00\rangle \pm |11\rangle$, where $|\Psi^{\pm}\rangle$ are negatively correlated and $|\Phi^{\pm}\rangle$ are positively correlated. Specifically in the context of frequency-bin encoding, our convention assigns logical state $|1\rangle$ to a higher frequency than the logical state $|0\rangle$ for each photon. We define two frequency bins in each of the signal and idler spectra and denote the Bell states as follows:

$$|\Psi^{\pm}\rangle = \frac{1}{\sqrt{2}} (|I_0 S_1\rangle \pm |I_1 S_0\rangle)$$

$$|\Phi^{\pm}\rangle = \frac{1}{\sqrt{2}} (|I_0 S_0\rangle \pm |I_1 S_1\rangle),$$
(4)

where I_n (S_n) denotes a single photon occupying a frequency bin centered at $\omega_{I,n} = \omega_{I,0} + n\Delta\omega$ ($\omega_{S,n} = \omega_{S,0} + n\Delta\omega$).

Following directly from energy conservation, the generation of $|\Psi^{\pm}\rangle$ states can be accomplished in a nonlinear parametric process that is activated by a monochromatic pump. Yet, the generation of $|\Phi^{\pm}\rangle$ states presents a more complex challenge. Here, we introduce a scheme for producing all frequency-bin Bell states via sequential driving of SPDC using single and dual spectral-line pumps. The single spectral line is used to obtain the negatively correlated Bell states $|\Psi^{\pm}\rangle$; dual spectral lines with suitable frequency separation are used to generate the positively correlated Bell states $|\Phi^{\pm}\rangle$. Efforts to generate the positively correlated Bell states $|\Phi^{\pm}\rangle$ via spontaneous four-wave mixing by dual spectral-line pumping of microrings in series have also been explored recently.²⁰

3.1 Setup

In our experimental design shown in Fig. 3(a), a continuous-wave laser centered at ~780.3 nm ($\omega_{p,0}/2\pi = 384.2 \text{ THz}$) is directed into an electro-optic intensity modulator (EOIM) which is controlled by a sinusoidal RF waveform at 25 GHz. The output generated by the EOIM is launched into fiber-pigtailed PPLN ridge waveguide that is designed for type-0 phase matching. Utilizing pulse shaper 1, two frequency bins with a width of 14 GHz each are selected on either side of the pump's half-frequency, with a separation of 25 GHz between them. The EOIM is configured to operate in one of two predetermined modes, resulting in the production of either a single or dual pump lines at its output. In the initial experiment, the RF input into the EOIM is attenuated to a negligible level to leave a single carrier at the output. From both the signal and idler spectra, two frequency bins with a separation of 25 GHz are extracted, i.e., $\{I_1, S_0\}$ and $\{I_0, S_1\}$ at offsets of ± 152.5 GHz and ± 177.5 GHz from $\omega_{p,0}/2$. The state of the biphotons generated in the two frequency bins takes the form $|\Psi^{(\alpha)}\rangle \propto |I_0S_1\rangle + e^{i\alpha}|I_1S_0\rangle$, with negative frequency correlations as shown in Fig. 3(b) where the phase α is contingent upon the difference in the time delays experienced by the entangled photons.

To generate $|\Phi^{\pm}\rangle$ states, the EOIM is configured to operate at carrier suppression by adjusting the DC bias to the null transmission point. This leads to the emergence of first-order sidebands, designated $\omega_{p,-1}$ and $\omega_{p,1}$, which are separated by 50 GHz as illustrated in Fig.3(c). The subsequent SPDC process generates time-energy

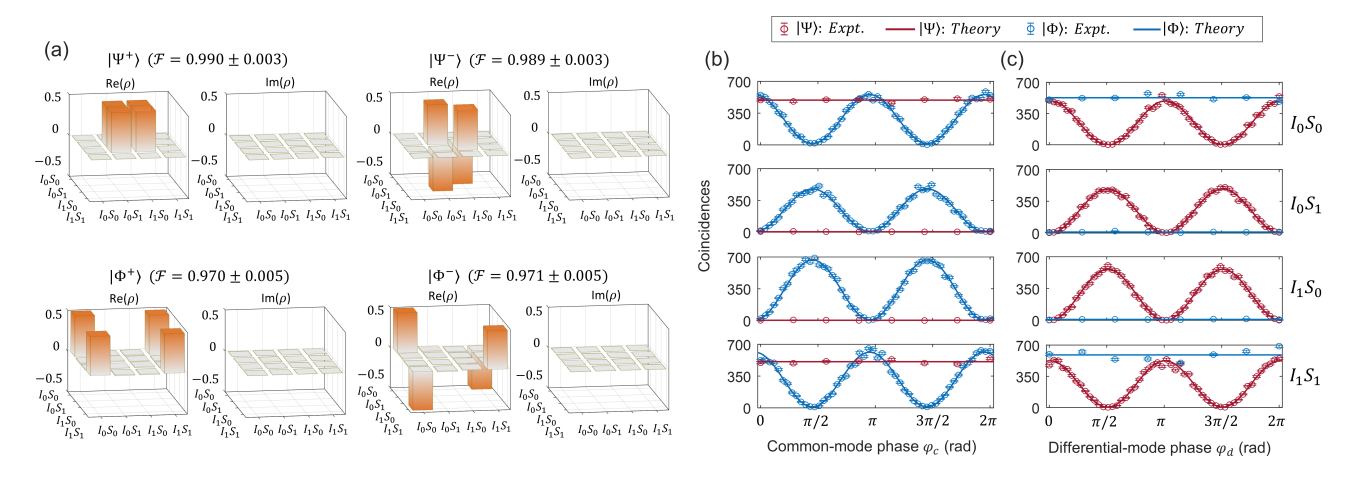


Figure 4. (a) Real and imaginary parts of Bayesian mean density matrices reconstructed for each of the Bell states from coincidence measurements. Coincidences acquired between different pairs of signal and idler bins as (b) differential-mode and (c) common-mode spectral phases are scanned following the application of Hadamard operation on the Bell states.

entangled photons in a coherent superposition of broadband spectral amplitudes centered at $\omega_{p,-1}/2$ and $\omega_{p,1}/2$. The frequency bins are again established with pulse shaper filters, resulting in the creation of a state of the form $|\Phi^{(\beta)}\rangle \propto |I_0S_0\rangle + e^{i\beta}|I_1S_1\rangle$, where the phase β originates from the RF modulation phase and mean optical delay of the biphotons.

3.2 Results and discussion

In these experiments, the phases α and β can be tuned by successively applying and scanning either a differential-mode phase φ_d on frequency bins I_1 and S_0 or a common-mode phase φ_c on the bins I_1 and S_1 , achieved by pulse shaper 1. Following this, parallel probabilistic Hadamard gates^{21, 22} are applied using an EOPM. To produce the four canonical Bell states, the phase α (β) is set to 0 for $|\Psi^+\rangle$ ($|\Phi^+\rangle$) or π for $|\Psi^-\rangle$ ($|\Phi^-\rangle$). The joint spectral intensities are then measured over all four pairs of logical idler and signal frequency bins, both with and without modulation from the EOPM—corresponding to measurements in the $Z \otimes Z$ and $X \otimes X$ Pauli bases, respectively. This information is used to recover their full density matrix via Bayesian inference, ^{23, 24} resulting in fidelities greater than $\geq 97\%$ for all Bell states as illustrated in Fig. 4(a). The results leveraging $|\Psi^+\rangle$ and $|\Phi^+\rangle$ for delay interferometry are depicted in Fig. 4(b,c). Here, α and β are set to zero and the EOPM is operated as a parallel Hadamard while the differential and common-mode phases (φ_d and φ_c) are sequentially applied and scanned. Coincidences registered for all the four bin-pair combinations { I_0S_0 , I_0S_1 , I_1S_0 , I_1S_1 } are plotted.

The application of common-mode phase φ_c on the bins S_1 and I_1 leaves $|\Psi^+\rangle$ unaltered by imparting only a global phase, but $|\Phi^+\rangle$ transforms into $|\Phi^{(2\varphi_c)}\rangle \propto |I_0S_0\rangle + e^{2i\varphi_c}|I_1S_1\rangle$. This transformation is equivalent to a common-mode delay (τ_c) experienced by the photons, where $\tau_c = (\tau_S + \tau_I)/2 = \varphi_c \Delta \omega^{-1}$, and τ_S (τ_I) is the total delay experienced by the signal (idler). We observe that entangled photons traveling through the same path accumulate a phase corresponding to twice the delay traversed, leading to a quantum enhancement by a factor of two.^{25,26} On the other hand, in the case of two unentangled photons, the enhancement in the sensing resolution as compared to that of a single photon is restricted to only $\sqrt{2}$, thereby highlighting the merit of entanglement-based sensing. From theory and experiment, the probability of coincidence detection between bins I_0S_0 and I_1S_1 is $\cos^2(2\varphi_c)$ while that for bin-pairs I_0S_1 and I_1S_0 is $\sin^2(2\varphi_c)$.

In contrast, the application of a differential-mode phase φ_d on the bins S_0 and I_1 leaves $|\Phi^+\rangle$ unchanged while transforming $|\Psi^+\rangle$ to $|\Psi^{(2\varphi_d)}\rangle \propto |I_0S_1\rangle + e^{2i\varphi_d}|I_1S_0\rangle$. This transformation is equivalent to a differential-mode delay experienced by each photon. The coincidence probability of the bin-pairs I_0S_0 and I_1S_1 is given by $\cos^2(2\varphi_d)$ while that for I_0S_1 and I_1S_0 is $\sin^2(2\varphi_d)$. The findings From Fig. 4(b,c) align with theoretical predictions, and demonstrate the versatility of our design in producing both classes of Bell states in a single setup, enabling capabilities in distributed sensing^{26,27} and measurements of delays and latencies in quantum networks, by leveraging the complementary aspects of frequency-bin Bell states.

4. CONCLUSION

In conclusion, we have presented a methodology for nonlocal delay metrology utilizing time-energy-entangled photons and, subsequently, have employed a technique for the generation of the complete Bell basis to showcase the sensitivities of Bell states with positive and negative frequency correlations to the sum and difference of entangled-photon delays. The proposed delay metrology approach can be implemented using readily available telecommunications equipment and standard quantum resources. Our work suggests the potential for utilizing high-dimensional entangled photons to directly sense important timing information and provide in-line synchronization data in an entanglement distribution system, potentially eliminating the control overhead associated with traditional classical synchronization techniques. Additionally, this sensing approach can be applied in ranging applications, where entanglement-based ToF measurements may provide superior performance compared to classical schemes in environments with high levels of ambient light or jamming signals.

Our second work on the generation of complete Bell basis offers practical advantages such as reduced complexity and lower insertion losses over prior schemes relying on unitary transformation from the negatively-to positively correlated Bell states by using a quantum frequency processor. Our experimental setup is characterized by its flexibility, as it can be easily reconfigured between single- and dual-line pump conditions, and utilizes passive spectral filtering. This allows for the synthesis of any Bell state within a fixed set of four frequency bins. Furthermore, the ability to switch between Bell states on-demand has potential applications in the field of quantum cryptography. ^{29–31}

ACKNOWLEDGMENTS

We thank AdvR for loaning the PPLN ridge waveguide and acknowledge Navin B. Lingaraju, Poolad Imany and Daniel E. Leaird for their contributions to the extended works summarized here. ^{16,17} Funding was provided by the National Science Foundation (1839191-ECCS, 2034019-ECCS) and the U.S. Department of Energy (ERKJ353). A portion of this work was performed at Oak Ridge National Laboratory, operated by UT-Battelle for the U.S. Department of Energy under contract no. DE-AC05-00OR22725.

REFERENCES

- [1] Lee, J., Shen, L., Cerè, A., Troupe, J., Lamas-Linares, A., and Kurtsiefer, C., "Symmetrical clock synchronization with time-correlated photon pairs," *Applied Physics Letters* **114**(10), 101102 (2019).
- [2] Giovannetti, V., Lloyd, S., Maccone, L., and Wong, F., "Clock synchronization with dispersion cancellation," *Phys. Rev. Lett.* **87**(11), 117902 (2001).
- [3] Ho, C., Lamas-Linares, A., and Kurtsiefer, C., "Clock synchronization by remote detection of correlated photon pairs," *New Journal of Physics* **11**(4), 045011 (2009).
- [4] Giovannetti, V., Lloyd, S., and Maccone, L., "Quantum-enhanced positioning and clock synchronization," *Nature* **412**(6845), 417–419 (2001).
- [5] Quan, R., Dong, R., Xiang, X., Li, B., Liu, T., and Zhang, S., "High-precision nonlocal temporal correlation identification of entangled photon pairs for quantum clock synchronization," Rev. Sci. Instrum. 91(12), 123109 (2020).
- [6] Zhao, J., Lyons, A., Ulku, A. C., Defienne, H., Faccio, D., and Charbon, E., "Light detection and ranging with entangled photons," Opt. Express 30(3), 3675–3683 (2022).
- [7] Liu, H., Giovannini, D., He, H., England, D., Sussman, B. J., Balaji, B., and Helmy, A. S., "Enhancing LIDAR performance metrics using continuous-wave photon-pair sources," *Optica* **6**(10), 1349–1355 (2019).
- [8] Frick, S., McMillan, A., and Rarity, J., "Quantum rangefinding," Opt. Express 28(25), 37118–37128 (2020).
- [9] Ren, X., Frick, S., McMillan, A., Chen, S., Halimi, A., Connolly, P. W., Joshi, S. K., Mclaughlin, S., Rarity, J. G., Matthews, J. C., et al., "Time-of-flight depth-resolved imaging with heralded photon source illumination," in [CLEO: Applications and Technology], AM3K.6, Optica Publishing Group (2020).
- [10] Lloyd, S., "Enhanced sensitivity of photodetection via quantum illumination," *Science* **321**(5895), 1463–1465 (2008).
- [11] Olislager, L., Cussey, J., Nguyen, A. T., Emplit, P., Massar, S., Merolla, J.-M., and Huy, K. P., "Frequency-bin entangled photons," *Phys. Rev. A* 82(1), 013804 (2010).

- [12] Kues, M., Reimer, C., Roztocki, P., Cortés, L. R., Sciara, S., Wetzel, B., Zhang, Y., Cino, A., Chu, S. T., Little, B. E., et al., "On-chip generation of high-dimensional entangled quantum states and their coherent control," *Nature* **546**(7660), 622–626 (2017).
- [13] Imany, P., Jaramillo-Villegas, J. A., Odele, O. D., Han, K., Leaird, D. E., Lukens, J. M., Lougovski, P., Qi, M., and Weiner, A. M., "50-GHz-spaced comb of high-dimensional frequency-bin entangled photons from an on-chip silicon nitride microresonator," Opt. Express 26(2), 1825–1840 (2018).
- [14] Imany, P., Odele, O. D., Jaramillo-Villegas, J. A., Leaird, D. E., and Weiner, A. M., "Characterization of coherent quantum frequency combs using electro-optic phase modulation," *Phys. Rev. A* **97**(1), 013813 (2018).
- [15] Imany, P., Lingaraju, N. B., Alshaykh, M. S., Leaird, D. E., and Weiner, A. M., "Probing quantum walks through coherent control of high-dimensionally entangled photons," *Sci. Adv.* **6**(29), eaba8066 (2020).
- [16] Seshadri, S., Lingaraju, N., Lu, H.-H., Imany, P., Leaird, D. E., and Weiner, A. M., "Nonlocal subpicosecond delay metrology using spectral quantum interference," *Optica* **9**(12), 1339–1346 (2022).
- [17] Seshadri, S., Lu, H.-H., Leaird, D. E., Weiner, A. M., and Lukens, J. M., "Complete frequency-bin Bell basis synthesizer," *Phys. Rev. Lett.* **129**, 230505 (2022).
- [18] Zhu, Z. and Wu, G., "Dual-comb ranging," Engineering 4(6), 772–778 (2018).
- [19] Trocha, P., Karpov, M., Ganin, D., Pfeiffer, M. H. P., Kordts, A., Wolf, S., Krockenberger, J., Marin-Palomo, P., Weimann, C., Randel, S., Freude, W., Kippenberg, T. J., and Koos, C., "Ultrafast optical ranging using microresonator soliton frequency combs," *Science* 359(6378), 887–891 (2018).
- [20] Clementi, M., Sabattoli, F. A., Borghi, M., Gianini, L., Tagliavacche, N., Dirani, H. E., Youssef, L., Bergamasco, N., Petit-Etienne, C., Pargon, E., Sipe, J. E., Liscidini, M., Sciancalepore, C., Galli, M., and Bajoni, D., "Programmable frequency-bin quantum states in a nano-engineered silicon device," Nat. Commun. 14, 176 (2023).
- [21] Imany, P., Odele, O. D., Alshaykh, M. S., Lu, H.-H., Leaird, D. E., and Weiner, A. M., "Frequency-domain Hong-Ou-Mandel interference with linear optics," *Opt. Lett.* **43**(12), 2760–2763 (2018).
- [22] Lu, H.-H., Simmerman, E. M., Lougovski, P., Weiner, A. M., and Lukens, J. M., "Fully arbitrary control of frequency-bin qubits," *Phys. Rev. Lett.* **125**(12), 120503 (2020).
- [23] Lukens, J. M., Law, K. J. H., Jasra, A., and Lougovski, P., "A practical and efficient approach for Bayesian quantum state estimation," New J. Phys. 22(6), 063038 (2020).
- [24] Lu, H.-H., Myilswamy, K. V., Bennink, R. S., Seshadri, S., Alshaykh, M. S., Liu, J., Kippenberg, T. J., Leaird, D. E., Weiner, A. M., and Lukens, J. M., "Bayesian tomography of high-dimensional on-chip biphoton frequency combs with randomized measurements," *Nat. Commun.* 13, 4388 (2022).
- [25] Giovannetti, V., Lloyd, S., and Maccone, L., "Quantum-enhanced measurements: beating the standard quantum limit," *Science* **306**(5700), 1330–1336 (2004).
- [26] Giovannetti, V., Lloyd, S., and Maccone, L., "Advances in quantum metrology," Nat. Photon. 5(4), 222–229 (2011).
- [27] Zhao, S.-R., Zhang, Y.-Z., Liu, W.-Z., Guan, J.-Y., Zhang, W., Li, C.-L., Bai, B., Li, M.-H., Liu, Y., You, L., Zhang, J., Fan, J., Xu, F., Zhang, Q., and Pan, J.-W., "Field demonstration of distributed quantum sensing without post-selection," *Phys. Rev. X* 11(3), 031009 (2021).
- [28] Lu, H.-H., Lukens, J. M., Peters, N. A., Williams, B. P., Weiner, A. M., and Lougovski, P., "Quantum interference and correlation control of frequency-bin qubits," *Optica* 5(11), 1455–1460 (2018).
- [29] Shi, R.-H. and Zhong, H., "Multi-party quantum key agreement with Bell states and Bell measurements," *Quantum Inf. Process.* **12**(2), 921–932 (2013).
- [30] Chun-Yan, L., Hong-Yu, Z., Yan, W., and Fu-Guo, D., "Secure quantum key distribution network with Bell states and local unitary operations," *Chin. Phys. Lett.* **22**(5), 1049 (2005).
- [31] Williams, B. P., Lukens, J. M., Peters, N. A., Qi, B., and Grice, W. P., "Quantum secret sharing with polarization-entangled photon pairs," *Phys. Rev. A* **99**(6), 062311 (2019).